Molecular basis of ancestral vertebrate electroreception

Nicholas W. Bellono[*], **Duncan B. Leitch**[*], and **David Julius**

Department of Physiology, University of California, San Francisco, California 94143, USA

Abstract

Elasmobranch fishes, including sharks, rays, and skates, use specialized electrosensory organs called Ampullae of Lorenzini to detect extremely small changes in environmental electric fields. Electrosensory cells within these ampullae are able to discriminate and respond to minute changes in environmental voltage gradients through an as-yet unknown mechanism. Here we show that the voltage-gated calcium channel $Ca_V1.3$ and big conductance calcium-activated potassium (BK) channel are preferentially expressed by electrosensory cells in little skate (*Leucoraja erinacea*) and functionally couple to mediate electrosensory cell membrane voltage oscillations, which are important in the detection of specific, weak electrical signals. Both channels exhibit unique properties compared with their mammalian orthologues to support electrosensory functions: structural adaptations in $Ca_V1.3$ mediate a low voltage threshold for activation, while alterations in BK support specifically tuned voltage oscillations. These findings reveal a molecular basis of electroreception and demonstrate how discrete evolutionary changes in ion channel structure facilitate sensory adaptation.

Sharks[1,2], weakly electric fishes[3], amphibians[4], and monotremes[5] can sense incredibly small electrical signals to communicate, detect prey, or navigate through the earth's electromagnetic field. Transduction of these electrical signals occurs through specialized electrosensory organs that differ in morphology and distribution through vertebrate lineages. Ancient electrosensory systems in elasmobranch fishes[1,2] such as the little skate (*Leucoraja erinacea*) detect electrical stimuli as small as 5 nV/cm through dermal pores that connect through low-resistance canals to specialized electrosensory cells within Ampullae of Lorenzini[1,2,6] (**Fig 1a-c**). Depolarization of electrosensory cells triggers neurotransmitter release onto afferent nerve fibers that project to the central nervous system[6,7,8]. Functional properties of ampullary organs have been described[7-11], but direct recordings from electrosensory cells are limited and biophysical properties of this unique sensory system are not well studied. Here, we identify a $Ca_V1.3$ voltage-gated calcium (Ca^{2+}) channel orthologue ($sCa_V1.3$) as the major voltage-gated cation channel in electrosensory cells of the little skate. $sCa_V1.3$ exhibits an unusually low voltage threshold, which is conferred by a

---

positively charged intracellular motif in the α_1 subunit. We show that sCa$_V$1.3 works in conjunction with a skate BK channel (sBK) that is molecularly adapted to support specific, behaviorally relevant voltage oscillation frequencies and amplitude[12-14], providing a mechanism for stimulus discrimination. Furthermore, treatment of behaving skates with Ca$_V$ and BK modulators substantiates roles for these channels in electroreception.

Cation currents in electrosensory cells

We obtained whole-cell patch-clamp recordings from dissociated electrosensory cells (**Fig. 1d**) using cesium (Cs$^+$) to block potassium (K$^+$) currents, thereby revealing a low-threshold voltage-activated inward current (**Fig. 1e**). This current (I$_{Cav}$) was blocked by nonspecific Ca$_V$ pore blockers (**Fig. 1f**), enhanced by the L-type agonist Bay K, and partially inhibited by L-type antagonists (**Fig. 1f**). I$_{Cav}$ was not affected by inhibitors of P/Q-, N-, or T-type Ca$_V$ channels, or by a Na$_V$ channel inhibitor (**Fig. 1f**). The conductance-voltage (G-V) relationship was steep with a relatively negative half maximal conductance compared with other Ca$_V$ channels[15]. Channel inactivation was slow, contributing to a large 'window current' representing sustained channel activity within a physiologically relevant voltage range (**Fig. 1g**). Thus, we conclude that I$_{Cav}$ is mediated by a low-threshold L-type Ca^{2+} channel with steep voltage dependence.

Previous electrophysiological recordings from little skate ampullary organs suggest that K$^+$ channels contribute to detection of weak electrical signals and membrane voltage oscillations, which are required for stimulus selectivity[7,8,10]. We measured K$^+$ currents directly using a K$^+$-based intracellular solution, revealing a large outward current in response to voltage pulses (**Fig. 1h**) that was blocked by the K$^+$ channel pore blocker TEA$^+$. Furthermore, pharmacological agents that modulated I$_{Cav}$ also regulated I$_K$ (**Fig. 1i**), suggesting that a Ca^{2+}-activated K$^+$ channel mediates I$_K$. Indeed, I$_K$ was blocked by selective inhibitors of BK channels, which are Ca^{2+}-activated (**Fig. 1h, i**).

Ca$_V$ and BK in electrosensory cells

To identify ion channel subtypes mediating I$_{Cav}$ and I$_K$, we transcriptionally profiled little skate ampullary organs. The orthologue of *cacna1d*, which encodes the α_1 subunit of Ca$_V$1.3, was the predominant Ca^{2+} channel subtype expressed in ampullae and greatly enriched (>90-fold) compared to other tissues examined (**Fig. 1j**). Several Ca$_V$ auxiliary subunits were also expressed (**Extended Data Fig. 1a**). Interestingly, mammalian Ca$_V$1.3 has a relatively low voltage threshold compared to other L-type Ca$_V$ channels, and plays a critical role in auditory hair cells, which are related to electrosensory cells[16-20]. We also examined expression profiles of pore-forming α subunits of K$^+$ channels and, consistent with our functional data, found that *kcnma1* (α subunit of BK) is the most abundant K$^+$ channel in ampullary organs, expressed at levels substantially higher (>35-fold) than other Ca^{2+}-activated K$^+$ channels (**Fig. 1j and Extended Data Fig. 1b**). At the cellular level, both Ca$_V$1.3 and BK transcripts were robustly expressed in ampullary receptor cells and absent in supporting cells and tubule structures (**Fig. 1k**). Expression of other Ca$_V$ and Ca^{2+}-activated K$^+$ channels was at or below the level of detection, but it remains possible that currents in electrosensory cells are not carried exclusively by Ca$_V$1.3 and BK.

sCa$_v$ has low voltage-activation threshold

The pore-forming subunit of sCa$_V$1.3 is 78% identical to the well-characterized long isoform of rat Ca$_V$1.3 (rCa$_V$1.3), and heterologous expression of sCa$_V$1.3 produced voltage-gated currents with ion sensitivity and pharmacological profiles resembling those of rCa$_V$1.3 or native electrosensory cell I$_{Cav}$ (**Extended Data Figs. 2 and 3**). However, like native I$_{Cav}$, the voltage threshold of sCa$_V$1.3 was significantly decreased compared to rCa$_V$1.3. Currents produced by sCa$_V$1.3 were activated at more negative potentials and increased steeply to maximal amplitude with increasing voltage (**Fig. 2a, b**). While inactivation was similar between sCa$_V$1.3 and rCa$_V$1.3, the G-V curve was significantly shifted in the negative direction for sCa$_V$1.3, contributing to a substantially larger window current for the skate channel (**Fig. 2c, d**). sCa$_V$1.3 also exhibited reduced Ca^{2+}-dependent inactivation compared to rCa$_V$1.3 (**Extended Data Fig. 2**). These functional properties match those of native I$_{Cav}$, suggesting that sCa$_V$1.3 forms the predominant voltage-gated Ca^{2+} channel in electrosensory cells.

What accounts for the decreased voltage threshold of sCa$_V$1.3? Measuring ionic and gating currents from the same cells allowed us to examine the relationship between relative conductance and voltage sensor movement (represented by ON gating charge, Q$_{ON}$) for skate versus rat orthologues. Both gating current kinetics and Q$_{ON}$-voltage relationships were similar (**Fig. 2e, f, and Extended Data Fig. 4a**); however, the G-V relationship was shifted to more negative voltages, and the Q$_{ON}$-G relationship was extremely steep for sCa$_V$1.3 compared with rCa$_V$1.3 (**Extended Data Fig. 4d**), suggesting that only minimal voltage sensor movement is required to elicit maximal channel opening for the skate channel (**Fig. 2f**). As another index of coupling efficiency, we measured maximal Q$_{ON}$ in the absence of pore blockers by applying voltage pulses to the channel's reversal potential (E$_{REV}$) and then stepping to –100mV to induce large tail currents (I$_{tail}$)[21]. Similar Q$_{ON}$ induced significantly larger I$_{tail}$ for sCa$_V$1.3 compared with rCa$_V$1.3 (**Fig. 2g**), suggesting that sCa$_V$1.3 exhibits greater channel open probability or open-state stability in response to equal voltage sensor movement. Collectively, these data indicate that the low voltage threshold of the skate channel originates from increased coupling between voltage sensors and channel opening.

Alignment of the α$_1$ subunit of sCa$_V$1.3 with human, rat, and zebrafish orthologues revealed a skate-specific insertion that introduces four positively charged residues (KKKER) into an intracellular loop of domain IV (DIVS2-S3) (**Fig. 3a**). Remarkably, a charge-neutralized mutant (neutral-sCa$_V$1.3; **Fig. 3a**) required significantly greater depolarization for maximal activation and exhibited decreased current density compared with WT-sCa$_V$1.3 (**Fig. 3b, c**). Gating current properties were not affected by charge neutralization (**Extended Data Fig. 4b, e**), but consistent with increased voltage threshold of neutral-sCa$_V$1.3, more relative Q$_{ON}$ was required for maximal conductance compared with WT-sCa$_V$1.3 (**Fig. 3d**). Furthermore, maximal Q$_{ON}$ elicited by voltage pulses to E$_{REV}$ resulted in decreased I$_{tail}$ amplitude in neutral-sCa$_V$1.3 versus WT-sCa$_V$1.3 (**Fig. 3e**). These results suggest that coupling between voltage sensor movement and channel opening is decreased in neutral-sCa$_V$1.3 and that the low voltage threshold of sCa$_V$1.3 is determined by the charged insertion in DIVS2-S3. Indeed, the charged motif from sCav1.3 (but not a neutralized

control) was sufficient to confer skate-like voltage sensitivity to rCa$_V$1.3,(**Fig. 3f, g**). Gating current properties of 'charged-rCa$_V$1.3' and 'neutral-rCa$_V$1.3' were similar (**Extended Data Fig. 4c, f**), but comparatively less relative Q$_{ON}$ was required for maximal conductance of charged-rCa$_V$1.3 and maximal Q$_{ON}$ elicited larger I$_{tail}$ (**Fig. 3h, i**), indicating enhanced coupling between voltage sensor movement and pore opening.

According to recent structural models of a related mammalian Ca$_V$[22], the charged skate motif within the intracellular loop of DIVS2-S3 could be relatively close to the bottom of the charged voltage sensor (DIVS4) such that electrostatic interactions could repel DIVS4 into a partially activated or primed state to decrease voltage threshold. To test this hypothesis, we examined voltage-dependent channel activation kinetics and found that activation occurred more rapidly in cells expressing charged-rCa$_V$1.3 compared with neutral-rCa$_V$1.3 or WT-rCa$_V$1.3 (**Extended Data Fig. 5a**). If charge interactions between the skate motif and DIVS4 position the voltage sensor in a primed state, then extremely negative voltages might force the voltage sensor into a resting state, resulting in activation kinetics similar to WT channels. Indeed, following a long negative prepulse (1 s, −170 mV), activation kinetics for charged-rCa$_V$1.3, neutral-rCa$_V$1.3 and WT-rCa$_V$1.3 were identical. As we increased the prepulse voltage to more positive values, the charged-rCa$_V$1.3 activation rate increased, while neutral-rCa$_V$1.3 and WT-rCa$_V$1.3 rates did not change (**Extended Data Fig. 5b, c**). These Cole-Moore shifts[23] demonstrate that an additional voltage-dependent step in channel activation occurs at very negative potentials in the presence of the charged skate motif, supporting our hypothesis that charge repulsion regulates the domain IV voltage sensor to decrease voltage threshold and enhance open-state stability at physiological membrane potentials (**Extended Data Fig. 5d**). Gating currents measure the movement of all voltage sensors (domains I–IV) irrespective of heterogeneity, thus a small difference, such as a partially activated voltage sensor, could be missed. While Cole-Moore effects support our model, further structural insights are required to confirm this hypothesis.

sBK has small conductance

We wondered if skate BK (sBK) is also specially adapted for electrosensation. Single-channel recordings from HEK293 cells expressing the α subunit (*kcnma1*) of skate or mouse BK showed that sBK had drastically reduced current amplitude at all voltages compared with mBK, resulting in a markedly decreased slope conductance (**Fig. 4a**). Both channels were similarly sensitive to intracellular Ca^{2+} (**Extended Data Fig. 6a**), but sBK single-channel currents were of smaller amplitude and had shorter open-state dwell time (**Fig. 4b**) such that sBK passes significantly less current than mBK.

Considering its unique conductance profile, we aligned the pore region of sBK with that of mouse, rat, human, and zebrafish orthologues to reveal high conservation (~87% identical to mBK), with a few notable alterations within an intracellular region near the pore that affects channel conductance through electrostatic interactions with K$^+$ (**Fig. 5a**)[24-28]. To determine if the altered amino acids affect sBK properties, we converted arginine and/or alanine of sBK to match cognate residues of mBK. sR340S significantly affected both conductance and open-state dwell time, while the effect of sA347E was less pronounced (**Fig. 5b, c, d**). Remarkably, substitution of both amino acids (sBK-SE) produced a single-channel

conductance nearly identical to that of mBK, with open-dwell time akin to the mouse channel (**Fig. 5b, c, d and Extended Data Fig. 6b**). Conversely, these two amino acids from sBK were sufficient to convert mBK conductance and open-time to that of sBK (mBK-RA, **Fig. 5b, c, d and Extended Data Fig. 6b**).

We next asked if altered K^+ concentration near the pore accounts for the reduced conductance of sBK. When patches expressing wild-type and mutant BK channels were exposed to various concentrations of intracellular K^+ (140mM, 640mM, or saturating 3.14M), single-channel amplitude increased for all BK channels with increasing K^+ concentration, and sBK and mBK-RA exhibited the smallest current amplitude at 140mM and 640mM (**Fig. 5e**). Current amplitude was the same for all channels when exposed to a saturating K^+ concentration of (3.14M), indicating that the pore is intrinsically capable of passing the same current (**Fig. 5e**). Notably, in the presence of 640mM, sBK channels passed nearly as much current as sBK-SE or WT mBK in 140 mM (**Fig. 5e and Extended Data Fig. 6c**). Thus, adaptations in sBK alter intracellular electrostatics near the pore to decrease the apparent conductance by reducing local K^+ concentration by >500mM.

Voltage oscillations in electroreception

Membrane voltage (V_m) oscillations, previously described in ampullary epithelial current-clamp experiments, control neurotransmitter release from electrosensory cells onto postsynaptic nerve fibers[7,8,29]. Under our conditions, electrosensory cells had a resting V_m of ~-55 mV and exhibited small, low frequency voltage oscillations. Injecting current to bring the V_m to various potentials modulated oscillatory behavior (**Fig. 6a**). Because oscillations occur over voltages where $sCa_V1.3$-mediated I_{Cav} is activated, we plotted oscillation amplitude versus membrane voltage and overlaid the normalized window current of I_{Cav} (**Fig. 6b**). Interestingly, average oscillation amplitude increased with window current, suggesting that tonic I_{Cav} activity underlies the depolarization phase of electrosensory cell V_m oscillations. In the presence of TEA^+, current injection elicited prolonged depolarization (**Fig. 6c**), suggesting that sBK-mediated I_K contributes to V_m oscillations, potentially by restoring cells to a hyperpolarized state after the initial depolarization. Furthermore, spontaneous oscillatory behavior was significantly reduced by TEA^+ or nifedipine (**Figs. 6d**). Taken together, our data suggest that I_{Cav} and I_K couple to mediate V_m oscillations.

How might sBK properties affect functional coupling of the two channels? As expected from reduced sBK conductance and open time, intracellular Ca^{2+} elicited smaller whole-cell currents from HEK293 cells expressing sBK compared to sBK-SE or mBK (**Extended Data Fig. 7a, b**). Voltage pulses in cells coexpressing $Ca_V1.3$ and sBK also elicited smaller K^+ currents and decreased K^+ permeability compared with sBK-SE or mBK. Thus, sBK allows for relatively more Ca_V-mediated Ca^{2+} current, while sBK-SE- and mBK-mediated K^+ currents quickly occlude measurable Ca^{2+} current (**Extended Data Fig. 7c, d**).

To determine if sBK-specific properties are important in native electrosensory cells, we used the selective BK agonist NS11021 (NS)[30] to pharmacologically increase P_o and open-state dwell time, producing a BK channel that more closely resembles mBK (**Extended Data Fig. 8a**). In recordings from cells coexpressing $Ca_V1.3$ and sBK, or from native electrosensory

cells, NS increased outward current amplitude and shifted reversal potentials in the negative direction, indicating increased BK activity and K^+ permeability (**Extended Data Fig. 8b-d**). In current-clamp experiments from electrosensory cells, treatment with NS dramatically reduced voltage oscillation amplitude and increased frequency (**Fig. 6f, g**). The addition of iberiotoxin blocked oscillations, consistent with a requirement for BK channels in spontaneous electrosensory cell V_m oscillations (**Fig. 6f**). Thus, evolutionary tuning of BK decreases conductance and its activity controls V_m oscillation amplitude and frequency. We hypothesize that because Ca_V-mediated Ca^{2+} influx immediately activates a BK current to limit the Ca_V-mediated depolarization, a smaller BK current will more slowly return V_m to rest, thus supporting large amplitude, low frequency oscillation events.

Electrosensory cells likely contain a mechanism to dampen BK-mediated hyperpolarization, thus maintaining a membrane voltage where Ca_V could initiate another oscillation event. Indeed, the highest expressed transcript in ampullary organs is parvalbumin 8, a Ca^{2+}-binding protein implicated in V_m oscillations[31] that could chelate Ca_V-mediated Ca^{2+} influx to produce only brief BK activation (**Extended Data Fig. 9a**). Consistent with this hypothesis, a plasma membrane Ca^{2+}-ATPase is also highly enriched in ampullary organs, presumably to support persistent oscillations (**Extended Data Fig. 9b, c**).

To examine the relative contributions of $sCa_V1.3$ and sBK at an organismal level, we preincubated behaving skates with vehicle or with nifedipine to inhibit Cav1.3, NS to stimulate BK, or mibefradil, a T-type Ca_V antagonist that does not affect I_{Cav} (**Fig. 1f**). We then asked if they favored a zone in which a submerged dipole electrical stimulus was buried under a sand-covered surface **(Fig. 6h).** For each treatment condition, a startle response was subsequently measured to confirm that the drug did not generally affect mobility (**Extended Data Fig. 10**). While both untreated and mibefradil-treated skates spent a majority of their time in the vicinity of the hidden electrical stimulus, skates treated with nifedipine or NS spent significantly less time near the active electrode (**Fig. 6i**). These results are consistent with the notion that $Ca_V1.3$ and low-level BK activity are important for electroreception-related behaviors.

Discussion

Electroreception is an ancient sensory modality that has independently evolved multiple times to facilitate the detection of environmental electrical signals for predation, navigation, or communication[6]. Electrosensory systems in elasmobranch fishes are among the most sensitive, and we have therefore exploited this system to gain molecular insights into mechanisms underlying this unique sensory modality. Our results demonstrate that low-threshold $sCa_V1.3$ couples to sBK to produce electrosensory cell V_m oscillations. This is reminiscent of electrical resonance in evolutionarily-related auditory hair cells, which also contain ribbon synapses and use Ca_V and BK orthologues to produce V_m oscillations that regulate vesicle release dynamics, allowing for the coding of stimulus strength and frequency[32-37]. In some animals, auditory hair cell electrical resonance tuning similarly contributes to frequency selectivity for incoming auditory signals[38,39]. Considering the simplicity and flexibility of this tuning mechanism, physiological state-dependent posttranslational modifications in electrosensory cell transducers may provide a means to

tune V_m oscillations for selective electrical frequency detection of salient signals from the environment according to developmental maturation, reproductive state, or nutritional condition. Oscillating tuberous electrosensory organs in weakly electric fishes (e.g., Gymnotiformes and Mormyriformes) are functionally tuned to electromagnetic fields related to self-generated electric organ discharges[6]; whether these systems use similar molecular mechanisms remains to be determined.

Methods

Animals and cells

Male and female little skates (*Leucoraja erinacea*) were provided by the Marine Biological Laboratory (Woods Hole, MA) and their use was approved by the UCSF Animal Care and Use Committee. Animals used for cellular physiology experiments were euthanized with tricaine methanesulfonate (MS222, 1g/L). Hyoid capsules were removed on ice, and individual ampullae were dissected by cutting the canals and afferent nerve fibers. Ampullae were treated with papain for 2-3 mins and then electrosensory cells were mechanically dissociated over the recording chamber. Isolated electrosensory cells were identified by the presence of their large single kinocilium. HEK293T cells (ATCC) were grown in DMEM, 10% fetal calf serum, and 1% penicillin/streptomycin at 37°C, 5% CO_2. Cells were transfected using Lipofectamine 2000 (Invitrogen/Life Technologies) according to manufacturer's protocol. 1 μg of skate or rat *cacna1d* was co-expressed with 1 μg rat cacnb3, 1 μg rat cacna2d1, and 0.3 μg GFP. Mock transfection experiments (1 μg rat cacnb3, 1 μg rat cacna2d1, and 0.3 μg GFP, but no cacna1d) were performed as controls, in which no voltage-activated inward currents were observed. For BK experiments, 1 μg of skate or mouse kcnma1 was co-expressed with 0.3 μg GFP. Mock transfection experiments with 0.3 μg GFP were performed as controls. To enhance expression of wild-type and charge-neutralized skate $Ca_V1.3$, cells were transfected for 6 – 8 hrs and then incubated at 28°C for 3 – 4 days, plated on poly-L-lysine-coated coverslips, incubated for an additional 3 – 4 days at 28°C, and then used for experiments[40].

Molecular biology

Cacna1d and *kcnma1* from little skate ampullary organs were synthesized by Genscript (Piscataway, NJ). Rat *cacna1d*, *cacnb3*, and *cacna2d1* were gifts from Diane Lipscombe (Addgene plasmids 49332, 26574, 26575) and mouse *kcnma1* was from Larry Salkoff (Addgene plasmid 16195). *Cacna1d* mutagenesis was carried out and verified by Genscript (Piscataway, NJ). *BK* point mutations were induced using QuikChange Lightning site-directed mutagenesis kit (Agilent Genomics).

Electrophysiology

Recordings were carried out at room temperature using a MultiClamp 700B amplifier (Axon Instruments) and digitized using a Digidata 1322A (Axon Instruments) interface and pClamp software (Axon Instruments). Whole-cell recording data were filtered at 1 kHz and sampled at 10 kHz. Data were leak subtracted online using a P/4 protocol, and membrane potentials were corrected for liquid junction potentials. Single-channel data were filtered at 5 kHz and sampled at 50 kHz. Electrosensory cell recordings were made using borosilicate

glass pipettes polished to 8 – 10 MΩ. The extracellular solution was a modified "elasmobranch Ringer's solution" containing (mM): 250 NaCl, 6 KCl, 4 CaCl$_2$, 1 MgCl$_2$, 10 glucose, 5 HEPES, 360 urea, pH 7.6. Two intracellular solutions were used: for recording I$_{Cav}$ (mM): 250 CsMeSO$_4$, 1 MgCl$_2$, 11 Cs-EGTA, 10 HEPES, 30 sucrose, 360 urea, pH 7.6. For recording I$_K$ or membrane potential (mM): 250 K-gluconate, 1 MgCl$_2$, 11 K-EGTA, 10 HEPES, 30 sucrose, 360 urea, pH 7.6. For heterologous expression experiments in HEK293, recordings were made using pipettes polished to 3 – 4 MΩ. For Ca$_V$1.3 recordings, Intracellular solution contained (mM): 150 NMDGMeSO$_4$, 1 MgCl$_2$, 10 Cs-EGTA, 10 HEPES, 10 sucrose, pH 7.3. Extracellular solution for measuring ionic current contained (mM): 150 choline chloride, 5 CaCl$_2$, 1 MgCl$_2$, 10 HEPES, 10 glucose, pH 7.3. For measuring gating currents, CaCl$_2$ was replaced with MgCl$_2$ and pore blockers (500 μM Cd^{2+} and 200 μM La^{3+}) were added to the extracellular solution. During ion substitution experiments, Ca^{2+} was substituted for an equal concentration of Ba^{2+} or Sr^{2+}. For BK single-channel recordings, intracellular solution contained (mM): 136 K-gluc, 4 KCl, 1 K-EGTA, 1 HEDTA, 10 HEPES, 10 glucose, pH 7.3. Extracellular solution contained (mM): 136 K-gluc, 4 KCl, 1 MgCl$_2$, 10 HEPES, 10 glucose, pH 7.3. Heterologous BK whole-cell recordings used an intracellular solution containing (mM): 140 K-gluc, 1 MgCl$_2$, 0.1 K-EGTA, 10 HEPES, 10 sucrose, pH 7.2. Extracellular solution contained (mM): 140 NaCl, 5 KCl, 2 CaCl$_2$, 2 MgCl$_2$, 10 HEPES, 10 glucose, pH 7.4. Calculated concentrations of buffered Ca^{2+} added to intracellular solution were made using MaxChelator (C. Patton, Stanford University).

The pharmacological inhibitors or agonists Bay K (Tocris), nifedipine (Tocris), nimodipine (Tocris), ω-agatoxin (Tocris), ω-conotoxin (Tocris), TTX (Tocris), charybdotoxin (Alamone Labs), iberiotoxin (Alamone Labs), and NS11021 (Tocris) were dissolved in <1% vehicle (DMSO or water), which was used for a control. Ionic pore blockers stocks were made in standard extracellular solution and diluted before use. Unless stated otherwise, the following concentrations were used: 2 mM Co^{2+}, 100 μM Cd^{2+}, 1 μM Bay K, 10 μM nifedipine, 10 μM nimodipine, 300 nM ω-agatoxin, 1 μM ω-conotoxin, 5 μM mibefradil, 50 μM nickel (low concentration to block T-type Ca$_V$), 1 μM tetrodotoxin, 1 μM charybdotoxin, 100 nM iberiotoxin, 10 mM TEA$^+$ 10 μM NS11021. Pharmacological effects were quantified by differences in normalized current from the same cell following bath application of the drug (I$_{treatment}$ / I$_{control}$).

Unless stated otherwise, currents were measured in response to 200 ms voltage pulses in 10 mV increments from a −115 mV holding potential. G-V relationships were derived from I-V curves by calculating G: G = I$_{Ca}$ / (V$_m$-E$_{rev}$) and fit with a Boltzman equation. Voltage-dependent inactivation was measured during −20 mV voltage pulses following a series of 1 s prepulses ranging from −115 to 65 mV in 10 mV increments. Voltage-dependent inactivation was quantified as I / I$_{max}$, with I$_{max}$ occurring at the voltage pulse following a −115 mV prepulse. Q$_{ON}$ represents the integral of nonlinear ON-gating current measured during voltage pulses from a holding potential of −110 mV. Q$_{ON}$ was only quantified from cells with no ionic current. Q$_{ON}$ – I$_{tail}$ relationships were examined by applying short pulses to predetermined E$_{rev}$ for each cell from −100 mV and stepping back to −100 mV to induce large I$_{tail}$.

Transcriptome sequencing and analysis

Poly A+ RNA was extracted from the ampullae, ampullary tubules/canals, non-electroreceptor covered skin, and liver of an adult *L. erinacea* then was reverse transcribed using the SuperScript III kit (Invitrogen/Life Sciences). Sequencing libraries were prepared using the Illumina TruSeq Stranded mRNA Library Prep Kit according to the manufacturer's instructions. Libraries were sequenced on the Illumina Hi-Seq 4000 (V. C. Genomics Sequencing Lab, University of California, Berkeley) using 150 cycles of paired end reads, producing 20 to 30 million inserts for each sample.

Transcriptomes for each sample were assembled *de novo* using the Trinity suite (version 2.1.0). Sequences were aligned to the zebrafish protein database (NCBI assembly GRCz10) using the blastx tool from NCBI blast (version 2.2.31) using a maximum *E* value of 1×10^{-5}. Reciprocal blastx alignments (using zebrafish protein sequences that aligned to *L. erinacea* sequences) were performed to the human protein database. Estimates of relative abundance for differential expression comparisons were performed using the RSEM software package within Trinity. These values are reported as fragments per kilobase of exon per million fragments mapped (FPKM).

Whole mount preparations

L. erinacea embryos were removed from egg cases, euthanized with an overdose of MS-222 in artificial seawater, and fixed in 4% paraformaldehyde for at least 24 hours. The cartilage matrix and electroreceptor tubules were stained using Alcian Blue (20 mg Alcian Blue 8GX in 30 mL glacial acetic acid and 70 mL 100% ethanol) following previously published methods[41].

In situ hybridization histochemistry

Adult skates were euthanized with an overdose of MS-222 in artificial seawater and trans-cardially perfused with PBS followed by 4% PFA. The hyoid capsule, which contained the aveolae of the ampullary organs, was dissected and cryo-protected in 30% sucrose in PBS overnight. Cryostat sections (15 μm thick) were probed with digoxigenin-labeled cRNA for skate $Ca_V1.3$ and fluorescein-labeled cRNA for skate BK receptors. Probes were generated by T7/T3 *in vitro* transcription reactions using a 510 nucleotide fragment of $Ca_V1.3$ cDNA (nucleotides 4501 to 5011) and a 510 nucleotide fragment of BK cDNA (nucleotides 2934 to 3444). Hybridization was developed using anti-digoxigenin and anti-fluorescein Fab fragments, followed by incubation with Fast Red and streptavidin conjugated Dylight 488 (to probe for BK) according to published methods[42]. Following hybridization and detection, sections were coverslipped and co-stained with DAPI as a nuclear marker (Prolong Gold Antifade Mountant with DAPI; Invitrogen).

Behavioral analysis

In an isolated location and under normal lighting conditions, juvenile skates were placed in 250 mL of seawater or seawater with 5 μM nifedipine, 10 μM NS –11021, or 5 μM mibefradil for 30 minutes. Following incubation, skates were allowed to habituate for 10 minutes in an acrylic cylindrical tank (diameter = 28 cm) and were surrounded by a barrier blocking external visual cues. A DC dipole stimulus (18 μA over 5 mm), generated by

threading positive and negative ends of tin-plated copper wire (300 VH, 22 gauge, NTE Electronics, Inc.) into seawater filled Tygon tubing, was randomly positioned and obscured by the sand substrate in one of four circles (diameter = 5.5 cm), all equally spaced from the center of the tank (see Extended Data Fig. 10A). All skates were exposed to a plume of Mysis shrimp odorant originating in the center of arena in order to elicit predatory/feeding behavior. A digital video camera (Sony Handicam) positioned above the tank was used to record skate activity for 30 minutes. Trials in which the skate executed >3 large movements and remained visible above the sand substrate for the majority of the time were quantified. Time spent with the majority of the pectoral disc within the outlined circle containing the electrical stimulus was compared to time spent in all other outlined circular areas. Following 30 minutes of undisturbed observation, tactile startle responses were observed from skates in response to gentle taps of the lateral pectoral fins to verify normal movement capabilities. Startle responses were quantified as the distance moved following a straight line from the dorsal side center between the eyes in still frames captured before and after the elicited startle response.

Statistical analysis

Data were analyzed with Clampfit (Axon Instruments) or Prism (Graphpad). Data are represented as mean ± sem and n represents the number of cells. Data were considered significant if $p < 0.05$ using paired or unpaired two-tailed Student's t-tests or one- or two-way ANOVAs. All significance tests were justified considering the experimental design and we assumed normal distribution and variance, as is common for similar experiments. Sample sizes were chosen based on the number of independent experiments required for statistical significance and technical feasibility.

Data Availability Statement

Deep sequencing data that support the findings of this study have been archived in the Gene Expression Omnibus (GEO) database repository with accession code GSE93582. GenBank accession numbers for skate $Ca_V1.3$ α subunit and skate BK α subunit are KY355736 and KY355737, respectively.
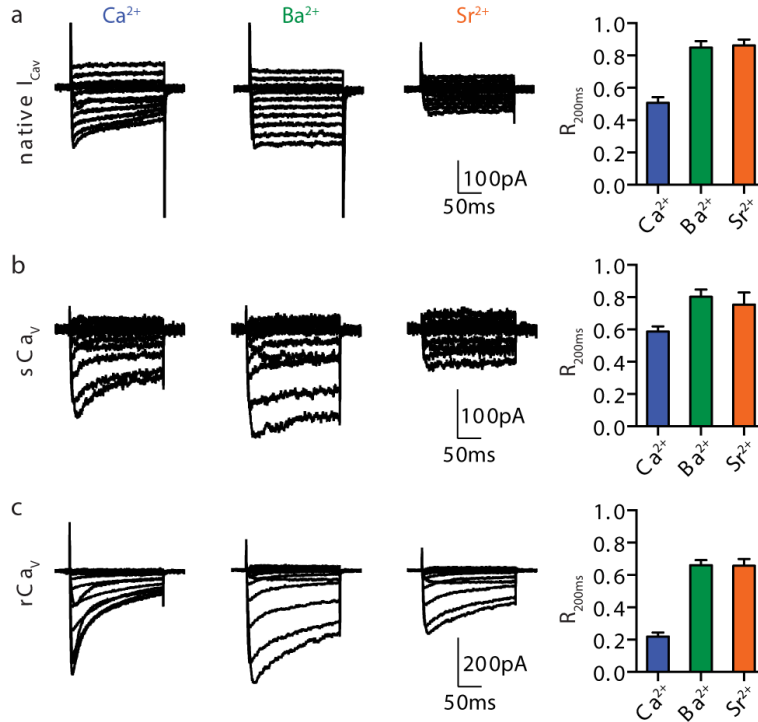
Extended Data
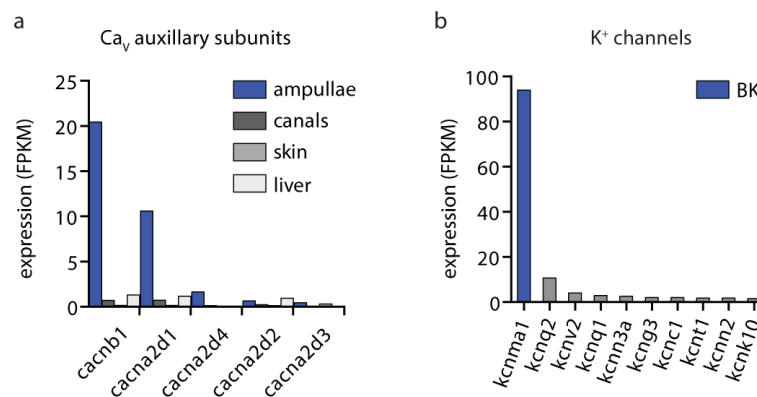
Extended Data Figure 1. Ca_V and K^+ channel expression in little skate

a. Ca_V auxiliary subunit mRNA expression in skate ampullary organs, ampullary canals, skin, and liver. Bars represent fragments per kilobase of exon per million fragments mapped (FPKM).

b. Ten most highly expressed K^+ channel α subunit transcripts in ampullary organs.

**Extended Data Figure 2. Skate Ca_V ion selectivity and Ca^{2+}-dependent inactivation**

a – c. Representative currents measured from electrosensory cells (native I_{CaV}, *top*), HEK293 expressing skate $Ca_V1.3$ (sCa_V, *middle*), or HEK293 expressing rat $Ca_V1.3$ (rCa_V, *bottom*) in the presence of 5 mM extracellular Ca^{2+}, Ba^{2+}, or Sr^{2+}. At the end of a 200 ms voltage pulse eliciting maximal current, approximately 50% of current remained in native electrosensory cell I_{Cav} or HEK293 cells heterologously expressing s$Ca_V1.3$, whereas r$Ca_V1.3$ had only ~20% current remaining. In electrosensory cells, heterologous s$Ca_V1.3$, or r$Ca_V1.3$, the percentage of remaining current was significantly increased by substituting extracellular Ca^{2+} for Ba^{2+} or Sr^{2+} ($p < 0.05$, one-way ANOVA with post-hoc Bonferroni test). Data represented as mean relative current remaining at the end of the 200 ms voltage pulses that elicited maximal currents ($\pm$ sem, n = 5 per condition).
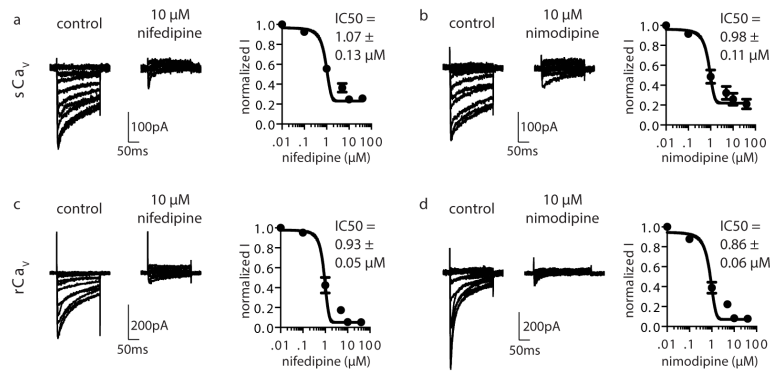
Extended Data Figure 3. Skate Ca$_V$ pharmacology

a – b. Pharmacology of skate Ca$_V$1.3 (sCav). Representative currents recorded in responses to voltage pulses in the presence of vehicle (control, <0.1% DMSO) or 10 μM nifedipine or nimodipine. Currents were incompletely inhibited similar to native electrosensory cell I$_{Cav}$ (**Fig. 1e**). Dose response relationships of current amplitudes measured at voltages that elicited maximal currents. Data are represented as mean ± sem, n = 6 per treatment.

c – d. Pharmacology of rat Ca$_V$1.3 (rCa$_V$). Representative currents in the presence of vehicle or 10 μM nifedipine or nimodipine and associated dose-response relationships. n = 6 per treatment.
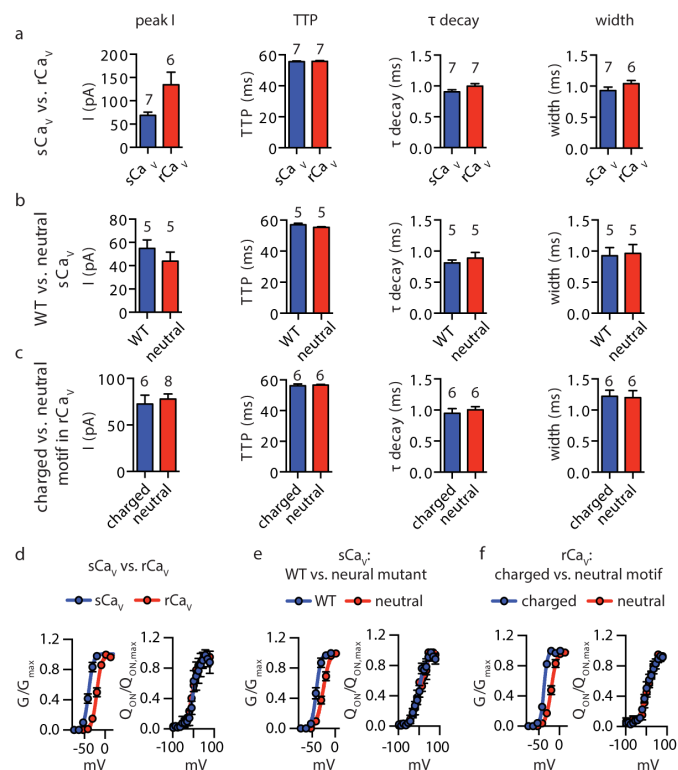
Extended Data Figure 4. Skate Ca$_V$ gating current properties

a – c. Gating current properties including peak amplitude (peak I), time-to-peak (TTP), exponential decay time constant (τ decay), peak width at 50% of maximal gating current

(width) for skate Ca$_V$1.3 (sCa$_V$) versus rat Ca$_V$1.3 (rCa$_V$, **a**, *top*), wild-type skate Ca$_V$1.3 (WT) versus charge-neutralized skate Ca$_V$1.3 (neutral, **b**, *middle*), and rat Ca$_V$1.3 with charged skate motif (charged) versus rat Ca$_V$1.3 with neutralized skate motif (neutral, **c**, *bottom*). All values were similar except for peak I for sCa$_V$ versus rCa$_V$, likely representing increased expression for rCa$_V$ compared with sCa$_V$. Data are presented as mean ± sem, n listed above bars.

d. Wild-type skate Ca$_V$1.3 (sCa$_V$, blue, n = 7) and wild-type rat Ca$_V$ (rCa$_V$, red, n = 8) relative conductance (G)-voltage (V) and ON-gating charge movement (Q$_{ON}$)-V relationships. Data represented as mean ± sem.

e. G-V and Q$_{ON}$-V relationships for wild-type sCa$_V$1.3 (WT, blue) and charge-neutralized sCa$_V$1.3 (neutral, red) relative conductance (G)-voltage (V) and ON-gating charge movement (Q$_{ON}$)-V relationships. Data represented as mean ± sem, n = 7 per condition.

f. G-V and Q$_{ON}$-V relationships for rCa$_V$1.3 with charged skate motif (charged, blue) and rCa$_V$1.3 with neutral skate motif (neutral, red). Data represented as mean ± sem, n = 8 per condition.
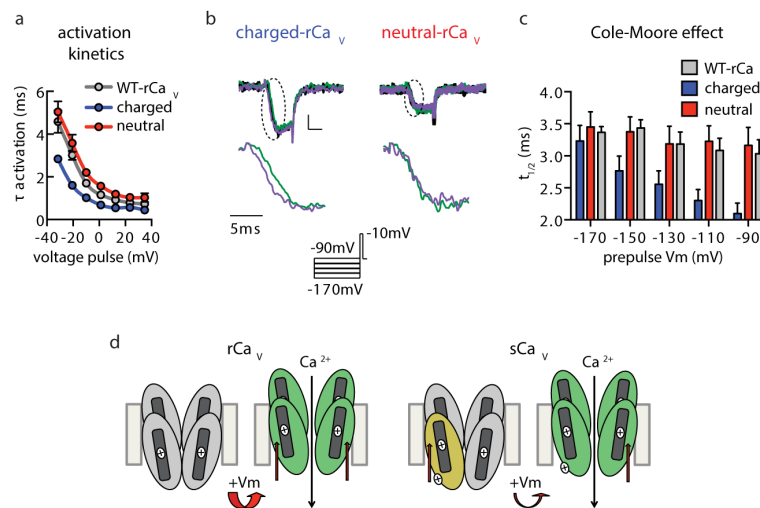

Extended Data Figure 5. Charged skate motif modulates voltage-dependent activation kinetics
a. Activation kinetics were faster in charged-rCa$_V$ (blue, n = 6) compared with wild-type rCa$_V$1.3 (WT-rCa$_V$, grey, n = 7) or neutral-rCa$_V$ (red, n = 8). Data represent mean ± sem, p < 0.05 at all voltages for charged-rCa$_V$ versus WT-rCa$_V$1.3 or neutral-rCa$_V$, two-way ANOVA with post-hoc Bonferroni test.
b. Representative currents recorded in response to 1 s voltage pulses between −170 and −90 followed by a pulse to −10 mV for 20 ms. Cole-Moore effects, indicated by increased current activation rate at −90 mV (purple) versus −170 (green), were observed in currents recorded from charged-rCa$_V$, but not in neutral-rCa$_V$ motif. Scale bar: 50 pA, 10 ms.
c. Cole-Moore effects quantified as the time to reach half maximal current (t$_{1/2}$). With increasing voltage during prepulses, charged-rCa$_V$ (blue, n = 9) reached maximal current amplitude faster while WT-rCa$_V$ (grey, n = 6) and neutral-rCa$_V$ (red, n = 8) were unchanged. All data represented as mean ± sem, n ≥ 7, p < 0.05 for charged-rCa$_V$ t$_{1/2}$ comparing −170 with −130, −110, or −90 mV, two-way ANOVA with post-hoc Bonferroni test).

d. Hypothetical model depicting the intracellular charged motif in the domain IV voltage sensor of sCa$_V$1.3 destabilizing the inactive state of the channel by electrostatic repulsion, pushing it into a partially activated or primed state (gold oval) prior to full activation (green ovals). Because sCa$_V$1.3 is primed for activation, channel activation requires a smaller increase in voltage compared with rCa$_V$1.3.
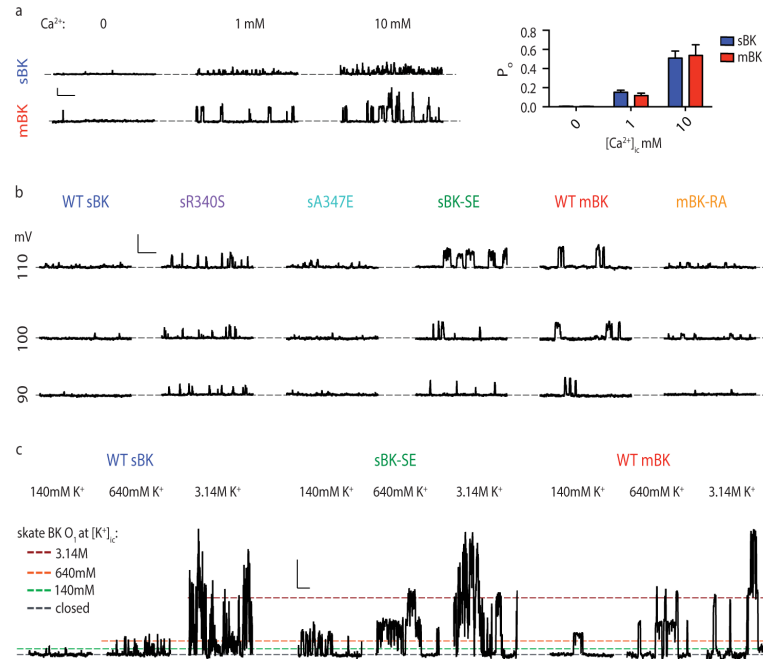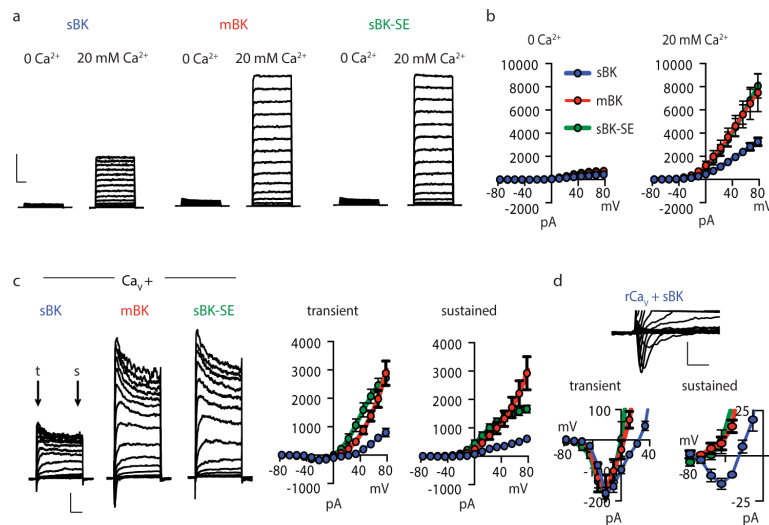

Extended Data Figure 6. Skate BK properties

a. Currents measured in response to 0, 1, or 10 μM intracellular Ca^{2+} at 80 mV from patches expressing sBK or mBK. Scale bar: 10pA, 50ms. Average open probability (P$_o$) for sBK compared with mBK was similar for all concentrations tested. Data represented as mean ± sem, n = 5.

b. Representative single-channel records at various voltages from patches expressing indicated BK channels. Scale bar: 25pA, 20ms.

c. Representative currents recorded at 80 mV from patches expressing indicated BK channels. The same patch was exposed to local K$^+$ concentrations of 140 mM, 640 mM, or 3.14 M. Dashed lines indicate single-channel current amplitude for sBK at 140 mM (green), 640 mM (orange), or 3.14 M (red). Scale bar: 50pA, 20ms.

Extended Data Figure 7. Adaptations in skate BK promote increased relative I_{CaV} current during channel coupling

a. Whole-cell currents in response to 200 ms voltage pulses from −80mV to +80mV from HEK293 expressing sBK, sBK-SE, or mBK in the presence of 0 or 20 μM intracellular Ca^{2+}. Scale bar: 5nA, 50ms

b. Average I-V relationships for sBK (blue), sBK-SE (green) or mBK (red) in the presence of 0 or 20 μM intracellular Ca^{2+}. n = 7.

c. Whole-cell currents from HEK293 expressing charged-$rCa_V 1.3$ coexpressed with sBK, sBK-SE, or mBK. Scale bar: 500pA, 50ms. t = transient current evoked by voltage pulse, s = sustained current. In the presence of $Ca_V 1.3$, average transient and sustained current-voltage relationships showed a negative shifted reversal potential (E_{REV}) for sBK-SE (green) or mBK (red) compared with sBK (blue), indicating increased relative K^+ permeability.

d. Reversal potentials for transient and sustained currents evoked in cells coexpressing charged-$rCa_V 1.3$ and BK were affected by BK identity. *Inset*: transient currents mediated by coupling of $Ca_V 1.3$ and BK (scale bar: 100pA, 5ms). Transient E_{REV}: sBK = 32.96 ± 2.17, mBK = 8.43 ± 2.76, sBK-SE = 3.42 ± 2.38, p < 0.0001 for sBK versus mBK or sBK-SE. Sustained E_{REV}: sBK = −17.00 ± 2.48, mBK = −50.95 ± 4.16, sBK-SE = −45.13 ± 4.59, p < 0.0001. n = 10. All data represented as mean ± sem and p values from two-tailed Student's t-test.
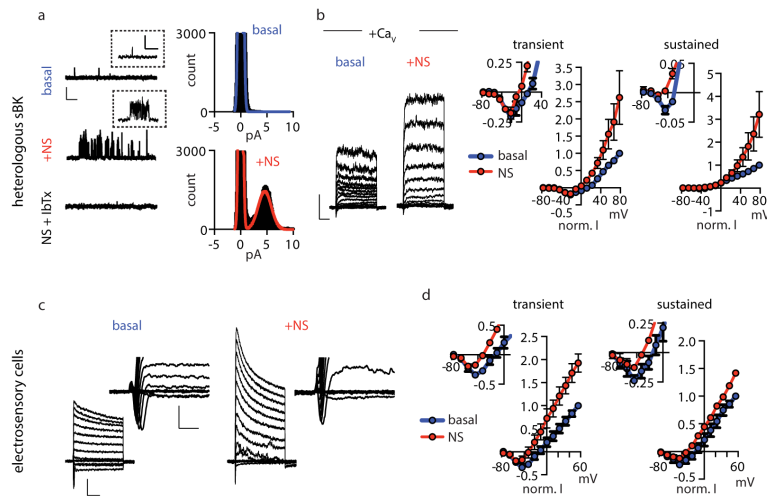
Extended Data Figure 8. BK agonist NS11021 modulates skate BK channels

a. In representative records from outside-out patches expressing sBK the BK agonist NS11021 (NS, 10 μM) increased the Po and open-state dwell time of sBK channels and this effect was blocked by iberotoxin (IbTx, 100 nM). Scale bar: 5pA, 100ms. Associated all-points histograms demonstrate the increase in open time. P_o: basal = 0.0024 ± 0.00068, NS: 0.16 ± 0.041, NS + IbTx = 0.00036 ± 0.00025, $p < 0.0001$ for NS versus basal or NS + IbTx. Open dwell time: 0.62 ± 0.32, NS: 4.59 ± 0.34, NS + IbTx = 0.30 ± 0.010, $p < 0.0001$. n = 5.

b. Whole-cell currents and average transient and sustained current-voltage relationships from HEK293 expressing charged-rCa$_V$1.3 and sBK (scale bar: 500pA, 50ms). Transient and sustained current-voltage relationships made from normalizing currents in the presence of NS to basal currents show an increase in Ca$_V$1.3-activated sBK current amplitude and negative-shifted E_{REV} in response to 10 μM NS. Transient E_{REV}: basal = 20.71 ± 3.46, +NS = -0.72 ± 0.94, $p < 0.01$. Sustained E_{REV}: basal = -24.62 ± 0.61, NS = -47.21 ± 5.37, $p < 0.05$. n = 5.

c. Representative currents recorded from an electrosensory cell show that 10 μM NS increases I_{Cav}-activated I_K amplitude resulting in a decrease in relative I_{Cav} current (scale bars: 100pA, 50ms).

d. Transient and sustained current-voltage relationships from normalizing currents in the presence of NS to basal currents. I-V relationships demonstrate an NS-mediated negative shift in E_{REV}, indicating increased K$^+$ permeability. Transient E_{REV}: basal = -6.15 ± 5.95, +NS = -24.9 ± 8.23, $p < 0.01$. Sustained E_{REV}: basal = -7.59 ± 6.02, NS = -26.65 ± 1.06, $p < 0.05$. n = 4. All data represented as mean ± sem and p values from two-tailed Student's t-test.
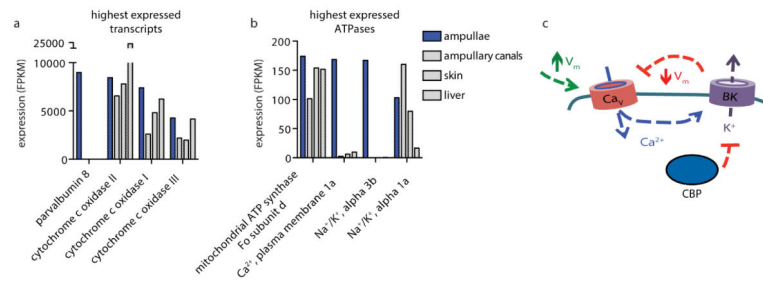
Extended Data Figure 9. Ca^{2+}-handling proteins are enriched in Ampullae of Lorenzini
a. Top 4 highest expressed transcripts in ampullae. The Ca^{2+}-binding protein (CBP) parvalbumin 8 is the highest expressed and is enriched in ampullae compared with other examined tissues. Bars represent fragments per kilobase of exon per million fragments mapped (FPKM).
b. Top 4 highest expressed ATPase transcripts in ampullae. Notably, the plasma membrane Ca^{2+} ATPase 1a is highly expressed and is enriched in ampullae.
c. Proposed mechanism for electrosensory cell V_m oscillations. sCa$_V$1.3 is activated by low threshold electrical signals to depolarize the cell and mediate Ca^{2+} influx. Ca^{2+} stimulates sBK-mediated K$^+$ current to hyperpolarize the cell. Ca^{2+}-binding proteins (CBP) bind incoming Ca^{2+} to inhibit BK-mediated hyperpolarization and continue sCa$_V$1.3-driven oscillations.
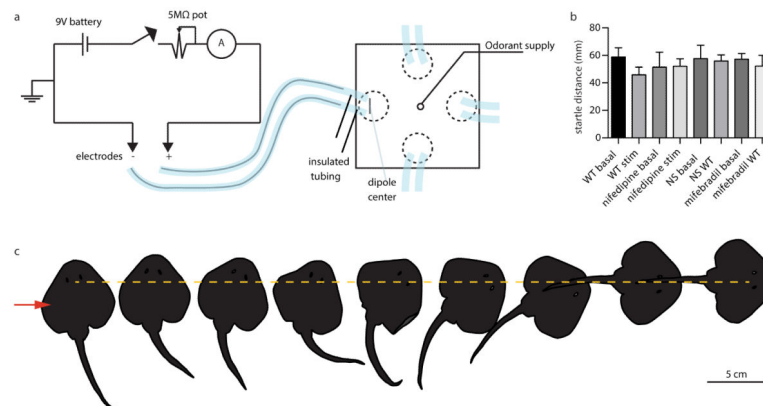
Extended Data Figure 10. Behavioral paradigm for pharmacologically-treated skates and startle response-related control
a. Schematic drawing of electrical stimulus. A 9V battery was used to generate a dipole DC stimulus through two independent leads placed into Tygon rubber tubing filled with seawater (left). The ends of these tubes were threaded through an acrylic plate to 4 different equally spaced locations on the base of the behavioral observation tank which were then obscured by sand (right).
b. Following 30 minutes of free exploration, control and pharmacologically-treated skates were gently tapped upon the pectoral fin. The average distance moved during the startle response is represented as mean ± sem; n=10. Differences were not significant according to a two-way ANOVA with post-hoc Tukey's test.
c. Schematic drawing traced from typical example of skate startle response following pectoral fin stimulation (red arrow). The distance covered during the startle response was

measured from the initial location (left) to the final location where the body axis became straight again (right), and the distance from the center between the eyes from each respective position was recorded (dotted yellow line).

Acknowledgments

References

1. Kalmijn AJ. The electric sense of sharks and rays. The Journal of Experimental Biology. 1971; 55:371–383. [PubMed: 5114029]

2. Kalmijn AJ. Electric and magnetic field detection in elasmobranch fishes. Science. 1982; 218:916–918. [PubMed: 7134985]

3. Lissmann HW, Machin KE. The mechanism of object location in Gymnarchus niloticus and similar fish. Journal of Experimental Biology. 1958; 35:451–486.

4. Munz H, Claas B, Fritzsch B. Electroreceptive and mechanoreceptive units in the lateral line of the axolotl Ambystoma mexicanum. J Comp Physiol. 1984; 154:33–44.

5. Scheich H, Langner G, Tidemann C, Coles RB, Guppy A. Electroreception and electrolocation in platypus. Nature. 1986; 319:401–402. [PubMed: 3945317]

6. Bullock TH. Electroreception. Annual Review of Neuroscience. 1982; 5:121–170.

7. Clusin WT, Bennett MV. The ionic basis of oscillatory responses of skate electroreceptors. The Journal of General Physiology. 1979; 73:703–723. [PubMed: 479811]

8. Clusin WT, Bennett MV. The oscillatory responses of skate electroreceptors to small voltage stimuli. The Journal of General Physiology. 1979; 73:685–702. [PubMed: 479810]

9. Peters RC, Zwart R, Loos WJG, Bretschneider F. Transduction at electroreceptor cells manipulated by exposure of apical membranes to ionic channel blockers. Comp Biochem Phys C. 1989; 94:663–669.

10. Araneda RC, Bennett MVL. Electrical-Properties of electroreceptor cells isolated from skate ampulla of lorenzini. Biol Bull. 1993; 185:310–311. [PubMed: 27768408]

11. Lu J, Fishman HM. Ion channels and transporters in the electroreceptive ampullary epithelium from skates. Biophysical Journal. 1995; 69:2467–2475. [PubMed: 8599653]

12. Sisneros JA, Tricas TC, Luer CA. Response properties and biological function of the skate electrosensory system during ontogeny. J Comp Physiol A. 1998; 183:87–99. [PubMed: 9691481]

13. Tricas TC, Michael SW, Sisneros JA. Electrosensory optimization to conspecific phasic signals for mating. Neurosci Lett. 1995; 202:129–132. [PubMed: 8787848]

14. Baker CA, Huck KR, Carlson BA. Peripheral sensory coding through oscillatory synchrony in weakly electric fish. eLife. 2015; 4

15. Catterall WA, Perez-Reyes E, Snutch TP, Striessnig J. International Union of Pharmacology. XLVIII. Nomenclature and structure-function relationships of voltage-gated calcium channels. Pharmacol Rev. 2005; 57:411–425. [PubMed: 16382099]

16. Platzer J, et al. Congenital deafness and sinoatrial node dysfunction in mice lacking class D L-type Ca2+ channels. Cell. 2000; 102:89–97. [PubMed: 10929716]

17. Koschak A, et al. alpha 1D (Cav1.3) subunits can form L-type Ca2+ channels activating at negative voltages. J Biol Chem. 2001; 276:22100–22106. [PubMed: 11285265]

18. Xu W, Lipscombe D. Neuronal Ca(V)1.3alpha(1) L-type channels activate at relatively hyperpolarized membrane potentials and are incompletely inhibited by dihydropyridines. The Journal of Neuroscience. 2001; 21:5944–5951. [PubMed: 11487617]

19. Brandt A, Striessnig J, Moser T. CaV1.3 channels are essential for development and presynaptic activity of cochlear inner hair cells. The Journal of Neuroscience. 2003; 23:10832–10840. [PubMed: 14645476]

20. Modrell MS, Bemis WE, Northcutt RG, Davis MC, Baker CVH. Electrosensory ampullary organs are derived from lateral line placodes in bony fishes. Nat Commun. 2011; 2

21. Hulme JT, Yarov-Yarovoy V, Lin TW, Scheuer T, Catterall WA. Autoinhibitory control of the CaV1.2 channel by its proteolytically processed distal C-terminal domain. The Journal of Physiology. 2006; 576:87–102. [PubMed: 16809371]

22. Wu J, et al. Structure of the voltage-gated calcium channel Cav1.1 complex. Science. 2015; 350

23. Cole KS, Moore JW. Potassium ion current in the squid giant axon: dynamic characteristic. Biophysical Journal. 1960; 1:1–14. [PubMed: 13694549]

24. Fodor AA, Aldrich RW. Convergent Evolution of Alternative Splices at Domain Boundaries of the BK Channel. Annual Review of Physiology. 2009; 71:19–36.

25. Soom M, Gessner G, Heuer H, Hoshi T, Heinemann SH. A mutually exclusive alternative exon of slo1 codes for a neuronal BK channel with altered function. Channels. 2008; 2:278–282. [PubMed: 18719396]

26. King BL, Shi LF, Kao P, Clusin WT. Calcium activated K(+) channels in the electroreceptor of the skate confirmed by cloning. Details of subunits and splicing. Gene. 2016; 578:63–73. [PubMed: 26687710]

27. Brelidze TI, Niu X, Magleby KL. A ring of eight conserved negatively charged amino acids doubles the conductance of BK channels and prevents inward rectification. Proc Natl Acad Sci U S A. 2003; 100:9017–9022. [PubMed: 12843404]

28. Nimigean CM, Chappie JS, Miller C. Electrostatic tuning of ion conductance in potassium channels. Biochemistry. 2003; 42:9263–9268. [PubMed: 12899612]

29. Teeter JH, Bennett MVL. Synaptic transmission in the ampullary electroreceptor of the transparent catfish, Kryptopterus. J Comp Physiol. 1981; 142:371–377.

30. Bentzen BH, et al. The small molecule NS11021 is a potent and specific activator of Ca2+-activated big-conductance K+ channels. Molecular Pharmacology. 2007; 72:1033–1044. [PubMed: 17636045]

31. Schwaller B, et al. Prolonged contraction-relaxation cycle of fast-twitch muscles in parvalbumin knockout mice. The American Journal of Physiology. 1999; 276:C395–403. [PubMed: 9950767]

32. Sejnowski TJ, Yodlowski ML. A freeze-fracture study of the skate electroreceptor. J Neurocytol. 1982; 11:897–912. [PubMed: 7153788]

33. Zanazzi G, Matthews G. The molecular architecture of ribbon presynaptic terminals. Mol Neurobiol. 2009; 39:130–148. [PubMed: 19253034]

34. Lewis RS, Hudspeth AJ. Voltage- and ion-dependent conductances in solitary vertebrate hair cells. Nature. 1983; 304:538–541. [PubMed: 6603579]

35. Hudspeth AJ, Lewis RS. A model for electrical resonance and frequency tuning in saccular hair cells of the bull-frog, Rana catesbeiana. The Journal of Physiology. 1988; 400:275–297. [PubMed: 2458455]

36. Miranda-Rottmann S, Kozlov AS, Hudspeth AJ. Highly specific alternative splicing of transcripts encoding BK Channels in the chicken's cochlea Is a minor determinant of the tonotopic gradient. Mol Cell Biol. 2010; 30:3646–3660. [PubMed: 20479127]

37. Rosenblatt KP, Sun ZP, Heller S, Hudspeth AJ. Distribution of Ca2+-activated K+ channel isoforms along the tonotopic gradient of the chicken's cochlea. Neuron. 1997; 19:1061–1075. [PubMed: 9390519]

38. Fettiplace R, Fuchs PA. Mechanisms of hair cell tuning. Annu Rev Physiol. 1999; 61:809–834. [PubMed: 10099711]

39. Rutherford MA, Roberts WM. Frequency selectivity of synaptic exocytosis in frog saccular hair cells. Proc Natl Acad Sci U S A. 2006; 103:2898–2903. [PubMed: 16473940]

40. Senatore A, Boone AN, Spafford JD. Optimized transfection strategy for expression and electrophysiological recording of recombinant voltage-gated ion channels in HEK-293T cells. J Vis Exp. 2011

41. Gillis JA, Dahn RD, Shubin NH. Chondrogenesis and homology of the visceral skeleton in the little skate, Leucoraja erinacea. J Morphol. 2009; 270:628–643. [PubMed: 19117064]

42. Ishii T, Omura M, Mombaerts P. Protocols for two- and three-color fluorescent RNA in situ hybridization of the main and accessory olfactory epithelia in mouse. J Neurocytol. 2004; 33:657–669. [PubMed: 16217621]
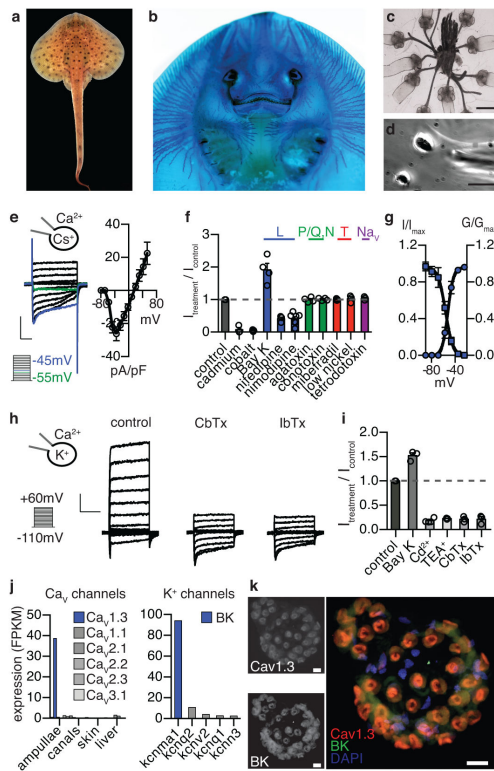
Figure 1. Ca$_V$1.3 and BK channels mediate the major cation currents in electrosensory cells

a. Dorsal profile of little skate (*Leucoraja erinacea*).

b. Alcian Blue-stained ampullary organ canals on the ventral surface of a juvenile skate.

c. Isolated ampullary organs with short lengths of canal and attached afferent nerve fibers (scale bar: 400 μm).

d. Electrosensory cells in a representative patch-clamp experiment (scale bar: 5 μm).

e. (*Left*) Representative I$_{Cav}$ traces: green and blue traces show current elicited by −55 and −45 mV pulse, respectively. (*Right*) Average current-voltage (I-V) relationship, n = 11. Scale bar: 20 pA/pF vertical, 100 ms horizontal.

f. Pharmacological profile of I$_{Cav}$. Channel subtype drug selectivity is indicated above bars. Each circle depicts one experiment; bars represent mean ± sem measured at peak amplitude; p < 0.05 for L-type channel modulators, one-way ANOVA with post-hoc Bonferroni test.

g. Conductance-voltage (G-V) relationship with half-maximal activation voltage (V$_{a1/2}$) of −52 ± 0.8 mV with slope factor (K$_a$) = 4.8 ± 0.6 mV. Inactivation-voltage relationship with half-inactivation potential (V$_{h1/2}$) of −55.9 ± 1.7 mV with slope factor (K$_i$) of −6.3 ± 1.6 mV. Window current was observed between −70 and −30 mV and peaks at ~-58 mV with ~40% maximal conductance. Data represented as mean ± sem, n = 10.

h. Representative K$^+$ currents. Scale bar: 20 pA/pF, 100 ms.

i. Pharmacological profile of I$_K$. Each circle depicts one experiment and bars represent mean ± sem measured at peak amplitude, p < 0.001 for control versus treatments, one-way ANOVA with post-hoc Bonferroni test.

j. (*Left*) Ca_v α subunit mRNA expression in skate ampullary organs, ampullary canals, skin, and liver. (*Right*) Expressed Ca^{2+}-activated K^+ channel α subunits in ampullary organs. Bars represent fragments per kilobase of exon per million fragments mapped (FPKM).

k. Co-localization of $Ca_V1.3$ (red) and BK (green) transcripts within electrosensory cells of ampullary organs visualized by *in situ* hybridization histochemistry. Nuclei were stained with DAPI (blue) Scale bar: 10 μm.
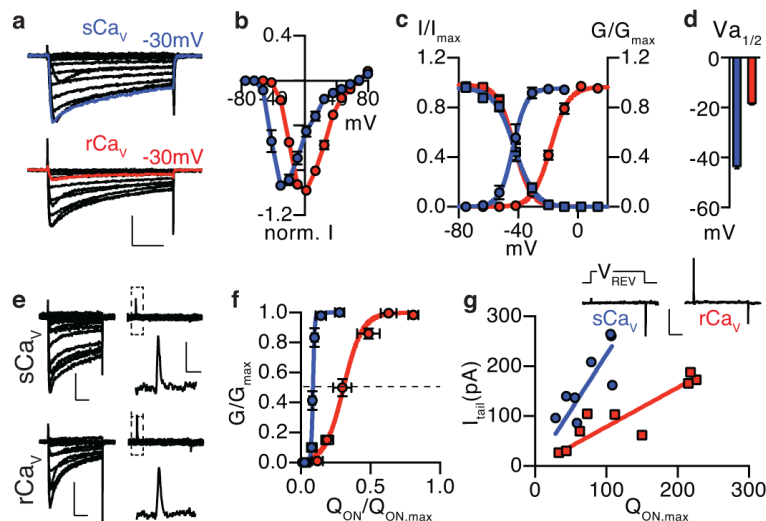
Figure 2. Skate Ca$_V$ has a low voltage threshold

a. Representative voltage-activated currents recorded in HEK293 expressing skate Ca$_V$1.3 (sCa$_V$, blue) or the homologous long isoform of rat Ca$_V$1.3 (rCa$_V$, red). Scale bar: 200 pA, 50 ms.

b. Normalized I-V relationship from sCa$_V$ (blue) and rCa$_V$ (red). n = 7.

c. sCa$_V$ (blue) and rCa$_V$ (red) G-V (n = 8) and inactivation (n =7) curves.

d. Average V$_{a1/2}$ for sCa$_V$ (-42.68 ± 0.56, n = 8) compared with rCa$_V$ (-18.16 ± 0.51, n = 7, p < 0.0001). V$_{h1/2}$ was similar, n = 7.

e. Ionic (*left*) and gating (*right*) currents from representative cells expressing sCa$_V$ or rCa$_V$. Scale bar for sCa$_V$: 100 pA, 50 ms; rCa$_V$: 200 pA, 50 ms. *Inset:* enlarged ON-gating currents. Scale bar: 50 pA, 3 ms.

f. Relationship of relative conductance (G / G$_{max}$, y-axis) and charge movement (Q$_{ON}$ / Q$_{ONmax}$, x-axis) for sCa$_V$ (blue, n = 7) and rCa$_V$ (red, n = 8). p < 0.0001 for difference in Q$_{ON}$ required for half maximal conductance (dashed line).

g. Maximal tail current (I$_{tail}$) versus maximal gating charge (Q$_{ON,max}$). Slopes: 2.23 ± 0.20 for sCa$_v$ (blue, n = 8), 0.79 ± 0.06 for rCa$_v$ (red, n = 9). *Inset:* representative ON-gating currents and I$_{tail}$ elicited by a voltage step to reversal potential (E$_{REV}$) from and returning to -100 mV. Scale bar: 100 pA, 50 ms. All data represented as mean $\pm$ sem, All p values from two-tailed Student's t-test.
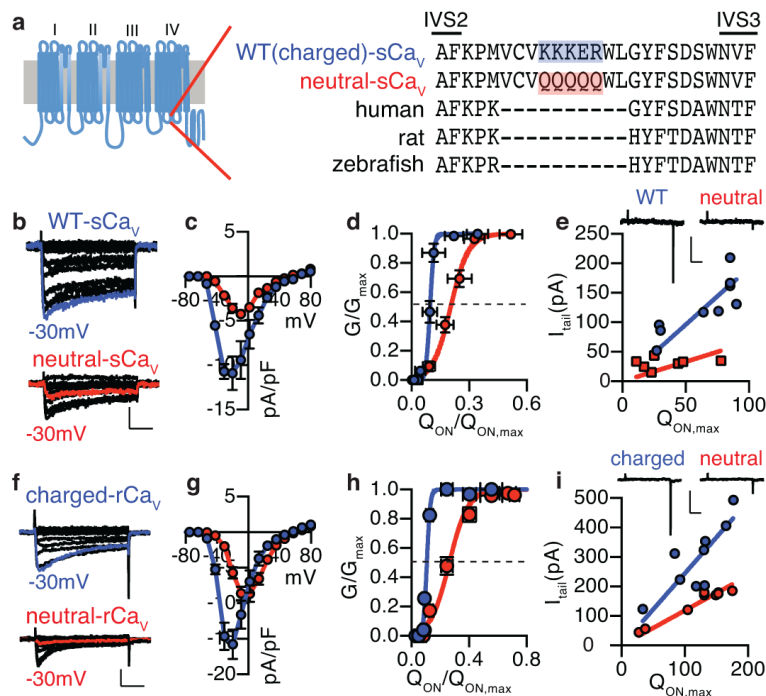
Figure 3. Positively charged motif confers skate Ca$_V$ voltage threshold

a. Predicted topology of Ca$_V$1.3 α_1 subunit. Species alignment reveals a positively charged insert in DIVS2-S3 of the skate orthologue. Charge-neutralized skate Ca$_V$1.3 (neutral-sCa$_V$) was generated by replacing charged residues (KKKER) of the skate motif with glutamines (QQQQQ).

b. Representative currents from HEK293 expressing wild-type skate Ca$_V$1.3 (WT-sCa$_V$, blue) or neutral-sCa$_V$ (red). Scale bar: 100 pA, 50 ms.

c. I-V relationships for WT-sCa$_V$ (blue) and neutral-sCa$_V$ (red). n = 7 per condition. V$_{a1/2}$ from WT-sCa$_V$ (-37.24 ± 0.32 mV) compared with neutral-sCa$_V$ (-25.99 ± 0.92 mV), n = 7 per condition, p < 0.0001).

d. G-Q$_{ON}$ relationship comparing neutral-sCa$_V$ (red) with WT-sCa$_V$ (blue).n = 7 per condition, p < 0.0001 for difference in Q$_{ON}$ required for half maximal conductance (dashed line).

e. I$_{tail}$ versus Q$_{ON,max}$. Slopes: 1.92 ± 0.15 for WT-sCa$_V$ (blue, n = 9), 0.66 ± 0.16 for neutral-sCa$_V$ (red, n = 7). *Inset:* representative maximal ON-gating currents and I$_{tail}$. Scale bar: 100 pA, 50 ms.

f. Representative currents from HEK293 expressing rCa$_V$1.3 with the charged skate motif (charged-rCa$_V$) or rCa$_V$1.3 with a neutralized skate motif insert (neutral-rCa$_V$). Scale bar: 100 pA, 50 ms.

g. I-V relationships for charged-rCa$_V$ (blue) and neutral-rCa$_V$ (red). n = 9 per condition. V$_{a1/2}$ from charged-rCa$_V$ (-37.24 ± 0.32 mV) compared with neutral-rCa$_V$ (-19.6 ± 0.32 mV), n = 9 per condition, p < 0.0001.

h. G-Q$_{ON}$ relationship comparing charged-rCa$_V$ (blue, n = 9) and neutral-rCa$_V$ (red, n = 8). p < 0.0001 for difference in Q$_{ON}$ required for half maximal conductance (dashed line).

i. I_{tail} versus $Q_{ON,max}$. Slopes: 2.45 ± 0.19 for charged-rCa$_V$ (blue), 1.19 ± 0.04 for neutral-rCa$_V$ (red). n = 9 per condition. *Inset:* representative maximal ON-gating currents and I_{tail}. Scale bar: 100 pA, 50 ms. All data represented as mean $\pm$ sem, All p values from two-tailed Student's t-test.
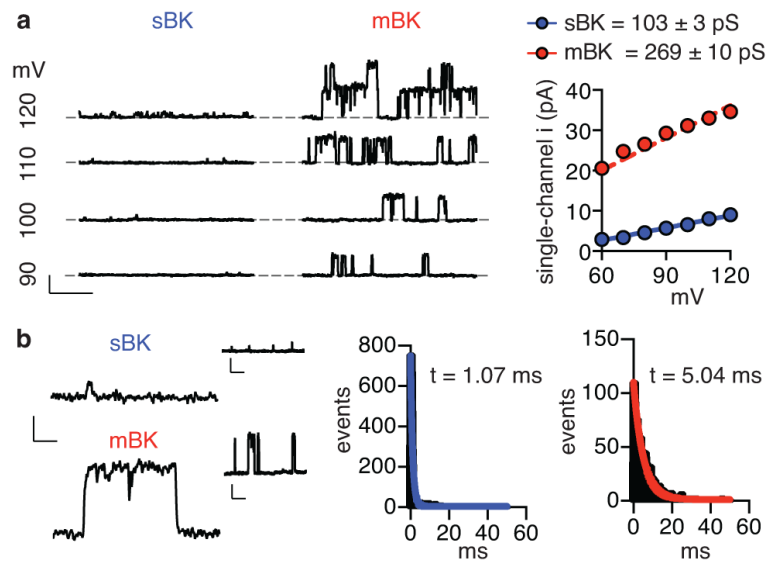
Figure 4. Skate BK has a small conductance and short open time
a. Representative sBK and mBK single-channel currents recorded at the indicated membrane voltages from excised patches from transfected HEK293 cells. Scale bar: 25pA vertical, 50ms horizontal. Average I-V relationship from sBK (blue) and mBK (red). n = 10 patches per condition, p < 0.0001 for difference in amplitude at each voltage.
b. Representative sBK or mBK single-channel kinetics recorded at 80mV. Scale bar: 10pA, 1ms. *Inset*: longer traces from same experiment (scale bar: 10pA, 50ms). Histograms of channel open times from 60s records fitted with a single-exponential to calculate open-state dwell time constants (sBK = 1.09 ± 0.02 ms, mBK = 5.06 ± 0.07 ms, n = 5, p <0.0001). All p values from two-tailed Student's t-test.
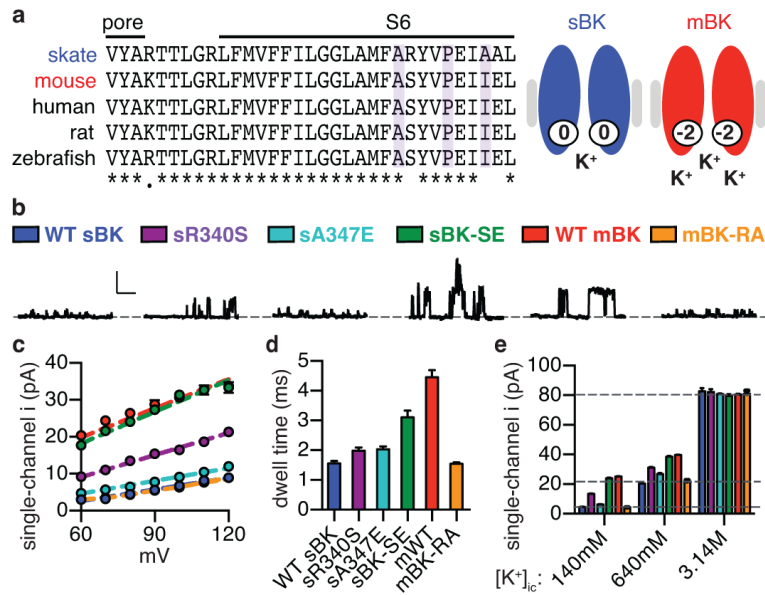
Figure 5. Intracellular electrostatic adaptations in the pore of skate BK

a. (*Left*) Species alignment of skate BK α subunit (*kcnma1*) reveals differences in charged residues. (*Right*) Net charge in this region determines local K^+ concentration and conductance of BK.

b. Representative single-channel records from patches at 120 mV expressing the indicated BK channels. Scale bar: 25pA, 20ms.

c. Average I-V relationship. Slope conductances: WT sBK (blue) = 104 ± 5.4 pS, sR340S (purple) = 200 ± 9.9 pS, sA347E (teal) = 115 ± 5.4 pS, sBK-SE (green) = 287 ± 14 pS, mBK (red) = 263 ± 15 pS, mBK-RA (orange) = 97 ± 3.6 pS. n = 5.

d. WT sBK and mBK-RA have significantly shorter open-state dwell times than all other BK channels tested (at 80 mV). $p < 0.001$, one-way ANOVA with post-hoc Tukey's test, n = 7.

e. Average single-channel amplitudes in response to changes in intracellular K^+ concentration. n = 5. Dashed lines indicate single-channel current amplitude for sBK at 140 mM (bottom), 640 mM (middle), or 3.14 M (top). All data represented as mean ± sem,
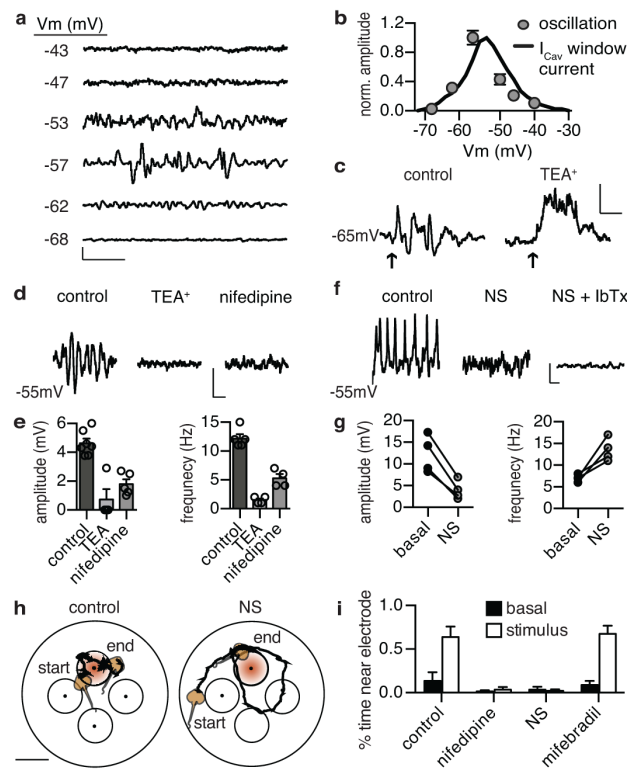
Figure 6. I_{Cav} and I_K tune voltage oscillations and electroreceptive behaviors

a. Representative traces showing membrane voltage-dependent oscillations at indicated membrane potentials (V_m). Scale: 5 mV, 500 ms.

b. Normalized amplitude of membrane voltage oscillations (from rest, averaged over 500 ms) at indicated V_m (n = 4). Overlaid normalized I_{Cav} window current (blue trace).

c. Current injection (10 pA, 5 ms at arrow) at −65 mV elicited oscillations or a sustained depolarization in the presence of TEA^+ (representative of n = 3). Scale bar: 5 mV, 100 ms.

d. Representative V_m oscillations were inhibited by TEA^+ or nifedipine. Scale bar: 5 mV, 100 ms.

e. Average oscillation amplitude and frequency. Each circle depicts one experiment; p < 0.001, one-way ANOVA with post-hoc Tukey's test.

f. V_m oscillations in response to NS11021 (NS) or NS + IbTx. Scale bar: 10mV, 250ms.

g. Average V_m oscillation amplitude and frequency. n = 4, p < 0.01 for amplitude, p < 0.05 for frequency, paired two-tailed Student's t-test.

h. Top down view of control (left) and NS11021-treated (NS, right) skates orienting towards a submerged electrical stimulus. Bolded line depicts movement from start time to end during 30 min trials. Scale bar: 5 cm.

i. Normalized percent time spent in area of submerged electrode for control, nifedipine, NS, and mifebradil-treated skates during basal condition or in the presence of an electrical stimulus. n = 10 trials for all conditions, p < 0.001 for control stimulus versus basal, p < 0.01 for control stimulus versus all treatments except mifebradil, two-way ANOVA with post-hoc Tukey's test. All data represented as mean ± sem.